coatings

MDPI

Article

Simulation of Dendrite Remelting via the Phase-Field Method

Xing Han, Chang Li *, Hao Zhan, Shuchao Li, Jiabo Liu, Fanhong Kong and Xuan Wang

School of Mechanical Engineering and Automation, University of Science and Technology Liaoning, Anshan 114051, China; hanxinggctx@163.com (X.H.)
* Correspondence: lichang2323-23@163.com

Abstract: The solidification of alloys is a key physical phenomenon in advanced material-processing techniques including, but not limited to, casting and welding. Mastering and controlling the solidification process and the way in which microstructure evolution occurs constitute the key to obtaining excellent material properties. The microstructure of a solidified liquid metal is dominated by dendrites. The growth process of these dendrites is extremely sensitive to temperature changes, and even a small change in temperature can significantly affect the growth rate of the dendrite tip. Dendrite remelting is inevitable when the temperature exceeds the critical threshold. In this study, a temperature-induced-dendrite remelting model was established, which was implemented through the coupling of the phase field method (PFM) and finite difference method (FDM). The transient evolution law of dendrite remelting was revealed by simulating dendritic growth and remelting processes. The phase field model showed that the lateral dendrites melt first, the main dendrites melt later, and the main dendrites only shrink but do not melt when the lateral dendrites have not completely melted or the root is not broken. The long lateral branches break into fragments, while the short lateral branches shrink back into the main dendrites. The main dendrites fracture and melt in multiple stages due to inhomogeneity.

Keywords: dendrite growth; phase field method; finite difference method; remelting

Citation: Han, X.; Li, C.; Zhan, H.; Li, S.; Liu, J.; Kong, F.; Wang, X. Simulation of Dendrite Remelting via the Phase-Field Method. *Coatings* **2024**, *14*, 1364. https://doi.org/10.3390/coatings14111364

Academic Editor: Avik Samanta

Received: 1 October 2024
Revised: 23 October 2024
Accepted: 24 October 2024
Published: 27 October 2024

1. Introduction

Solidification is a ubiquitous physical phenomenon observed in nature. During the processing of metallic materials—encompassing techniques such as casting, additive manufacturing, and welding—multiple solidification events typically occur, and it is common for a material to undergo one or more solidification processes [1–3]. Solidified molten metal liquid will form dendritic crystals [4]. The growth processes of these dendrites are exceedingly sensitive to temperature changes; even minor changes in temperature affect the growth rate of the tip of the dendrite significantly. A slight increase in temperature results in a deceleration of dendrite tip growth, whereas a slight decrease in temperature accelerates the tip growth rate. When the temperature rises beyond a critical threshold, the phenomenon of dendrite remelting becomes inevitable [5]. The dendrite remelting process is usually accompanied by the dynamic evolution of dendrite morphology, including the morphological reconstruction of the lateral and main dendrite arms, volume contraction, and local melting nonuniformity. This phenomenon exemplifies the intricate interplay of thermodynamic and kinetic behaviors during crystal growth and phase transformation processes. While dendrite remelting exerts a significant influence on alloy solidification structures, the majority of studies to date remain concentrated on macroscopic simulations and experimental microstructural characterization, with numerical modeling of this phenomenon being relatively underexplored.

Dendrite remelting is predominantly governed by two principal driving factors: solute-induced and temperature-induced mechanisms. Neng Ren et al. [6] successfully simulated dendritic growth and remelting under solute-induced conditions by employing a coupled

Cellular Automaton (CA) and Finite Volume Method (FVM). Their model takes into account critical conditions for mechanical fragmentation, alongside dendrite melting and fragmentation induced by convective flow and solute segregation. Peng Xialin et al. [7] employed a coupled phase field method (PFM) and finite difference method (FDM) to simulate and analyze dendritic growth and remelting under solute-induced conditions. Furthermore, this model accounted for the influence of lateral convection and linear flow velocity on the dendrite-remelting process. Previous research predominantly concentrated on solute-induced mechanisms as the primary driving factor, whereas numerical simulations exploring temperature-induced mechanisms remain relatively limited.

The phase field method (PFM) represents a computational method for accurately capturing phase transition interface dynamics throughout the solidification process [8]. At the macroscopic scale, phase transition problems such as solid-state phase transition and droplet phase fusion can be described by using a partial differential equation introduced into the interface [9]. At the microscopic scale, the physical state of the system phase in time and space over the growth domain Ω is described through the ordering parameter $\psi(r,t)$. In dendritic phase field models, the solid phase is typically assigned a $\varphi = 1$, the liquid phase is assigned a $\varphi = 0$, and the interfacial region is represented by $0 < \varphi < 1$ [10]. The PFM is based on the Ginzburg–Landau theory and describes the combined effects of ordering, interfacial diffusion, and thermodynamic driving through differential equations [11,12]. The PFM is also known as a direct simulation method that can track the solid–liquid interface and directly simulate the internal structure of dendrite growth, dendrite morphology, and other microstructures. The phase field method can perfectly solve the complex solid–liquid interface tracking problem, and it can also be coupled with the temperature field and solute field to enable quantitative studies on the growth and evolution of microstructures during metal solidification [13–15]. The finite difference method (FDM) is a commonly used numerical analysis method [16]. The core principle of the FDM involves discretizing the definition domain of a problem into a computational grid and subsequently applying suitable numerical differentiation formulas at the grid nodes to approximate the differential terms, thereby converting the continuous differential equations into the difference equations in discrete form. This process establishes a difference scheme, which is subsequently solved to derive the numerical solution of the original problem.

This study presents a novel temperature-induced dendrite-remelting model. The model was implemented by coupling the phase field method (PFM) with the finite difference method (FDM). The dendritic evolution process, encompassing both dendrite growth and remelting, was simulated, and the transient evolution law of dendrite remelting was revealed. These findings are of great significance for controlling the microstructure and mechanical properties of processed materials.

In summary, a temperature-induced-dendrite-remelting model is established in this paper. The model was implemented via the coupling of the phase field method (PF) and the finite difference method (FDM). The dendrite evolution process, including dendrite growth and dendrite remelting, was successfully simulated, and the transient evolution law of dendrite remelting is revealed herein, constituting findings of great significance for controlling the microstructure and mechanical properties of machined materials.

2. Phase Field Model

2.1. Establishment of Remelting Phase Field Model

Dendrite remelting is a phenomenon in which a dendrite originally in a stable growth state under the condition of an elevated ambient temperature undergoes a phase transition due to a change of temperature field. This results in the migration of its solid–liquid interface toward increasing the volume of the liquid phase, which triggers the localized or overall melting of the crystal [17]. To effectively describe the remelting process of dendrites, this study employs the non-isothermal phase field model, as derived by Kobayashi [18], Boettinger [19], and Zaeem [20]. In order to ensure the accuracy and stability of the numerical simulation, the following assumptions were made during the simulation of the

regrowth of remelted dendrites: (1) the driving force of temperature undercooling during the regrowth of remelted dendrites remained unchanged; (2) the regrowth of adjacent dendrites was restricted by the boundaries on both sides; and (3) the latent heat during dendrite regrowth remained constant. The governing equations for the phase field and temperature field in this model are presented as follows:

$$\frac{\tau_c}{\widetilde{\varepsilon}_m^2}\frac{\partial \psi}{\partial t} = \left[\frac{\partial}{\partial x}\left(\frac{\partial \varepsilon^2(\theta)}{\partial \theta}\frac{\partial \psi}{\partial y}\right) - \frac{\partial}{\partial y}\left(\frac{\partial \varepsilon^2(\theta)}{\partial \theta}\frac{\partial \psi}{\partial x}\right) + \nabla\cdot\left(\varepsilon^2(\theta)\psi\right)\right] + \frac{1}{\widetilde{\varepsilon}_m^2}\psi(1-\psi)\left[\psi - \frac{1}{2} + M\left(\widetilde{T}\right)\right] \quad (1)$$

$$\frac{\partial \widetilde{T}}{\partial t} = \alpha_T \nabla^2 \widetilde{T} + \frac{L_m}{C_p}\frac{\partial \psi}{\partial t} \quad (2)$$

where τ_c and $\widetilde{\varepsilon}_m$ are the interfacial parameters of the phase field, and $\varepsilon(\theta)$ is the anisotropy of each of the solid–liquid interfaces ($\varepsilon(\theta)$ is a function of θ, as given by Equation (3) [21]. $M(\widetilde{T})$ is the interface driving term in the phase field equation, where $M > 0$ for the solidified state and $M < 0$ for the melted state, and T_{ap} is the equilibrium temperature during solidification. α_T is the thermal diffusion coefficient of the metal, C_p is the constant pressure heat capacity, L_m is the latent heat, and $\widetilde{T}$ is the dimensionless temperature, wher e $\widetilde{T} = (T - T_S)/(T_L - T_S)$ [22]:

$$\varepsilon(\theta) = \overline{\varepsilon}\eta(\theta) = \overline{\varepsilon}(1 + \delta\cos(k_\varepsilon(\theta - \theta_0))) \quad (3)$$

$$\theta = \frac{\nabla\varphi}{|\nabla\varphi|} = \arctan\left(\frac{\partial\varphi/\partial y}{\partial\varphi/\partial x}\right) \quad (4)$$

$$M(T) = \left(\frac{\alpha}{\Pi}\right)\arctan\left(\sigma(T_{ap} - T)\right) \quad (5)$$

$$\alpha_T = \frac{l_0^2}{\tau} = \frac{k}{\rho C_p} \quad (6)$$

In the actual solidification process, the solid–liquid interface can be randomly undulated due to solute diffusion, heat flow, and other reasons [23,24]. In order to simulate such random interfacial fluctuations and make the dendrite growth more realistic, random perturbations were added to the phase field equations:

$$\frac{\partial \psi}{\partial t} \rightarrow \frac{\partial \psi}{\partial t} + 16 g'(\psi) a^{\#} r^* \quad (7)$$

where $g'(\psi)$ is the derivative of $g(\psi) = \psi^2(1-\psi)^2$, $\alpha^{\#}$ is the perturbation intensity factor (which is time-dependent), and r^* is a random number between -1 and +1. To ensure that the perturbation occurs at the interface, the effect of the noise term exists only in the range where $0 \le \psi \le 0.5$.

2.2. The Establishment of Geometric Model and the Determination of Boundary Conditions

The finite element computing platform was used to solve the numerical model in this study. According to the characteristics of the dendrite growth, taking into account the cost of the calculation, this section establishes a rectangular model, as shown in Figure 1. Figure 1a depicts the geometrical modeling of the competitive dendrite growth process, and overall mesh delineation was performed by using free triangles. The model contains 9040 cells and 260 boundary cells, with a minimum cell mass is 0.6885.

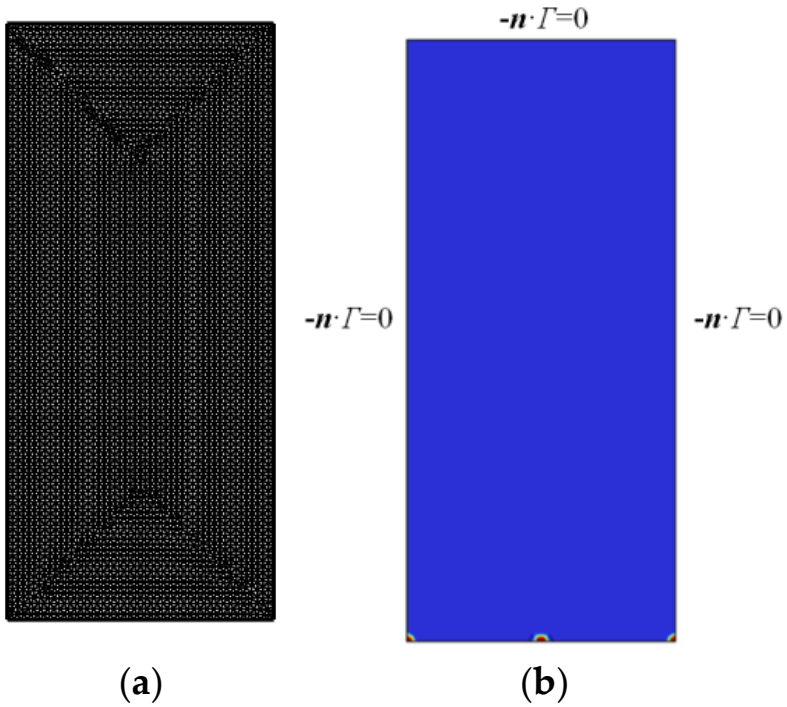

Figure 1. Modeling of dendrite remelting. (**a**) Dendrite-remelting model meshing. (**b**) Nucleation positions and boundary conditions for dendrite-remelting setups.

To ensure adequate spacing between crystal nuclei in the initial distribution, providing sufficient room for the growth of secondary dendrite arms, crystal nucleus positions were predefined at the base of the simulation domain. In solving the control equations of the phase field model, it was assumed that the crystal nucleus positions were influenced solely by growth kinetics, free from external interference. Consequently, zero-flux boundary conditions were imposed at the boundaries of the simulation domain, ensuring that both mass and energy transport were zero and preventing external factors from influencing the crystal growth process. This ensured that the simulation results more faithfully represent the actual dendritic growth mechanisms during the remelting process. The predefined crystal nucleus positions and boundary conditions are shown in Figure 1b.

3. Analysis of Dendrite-Remelting Simulation Results

3.1. Dendrite Remelting Process

Figure 2 shows the stable growth states of the dendrites prior to the rise in environmental temperature. As shown in Figure 2a, under the influence of the interface anisotropy, the crystal nucleus shows obvious main dendrite growth in both horizontal and vertical directions, showing the typical preferred orientation characteristics in the dendrite growth process. As shown in Figure 2b, due to the small distance between crystal nuclei in the simulation domain, the main dendrites of adjacent dendrites in the horizontal direction are limited by the competitive behavior of adjacent crystals, resulting in their growth inhibition. However, in the vertical direction, the main dendrites can fully grow along this direction due to the small influence of space limitation, thus exhibiting an obvious growth morphology extending along the vertical direction.

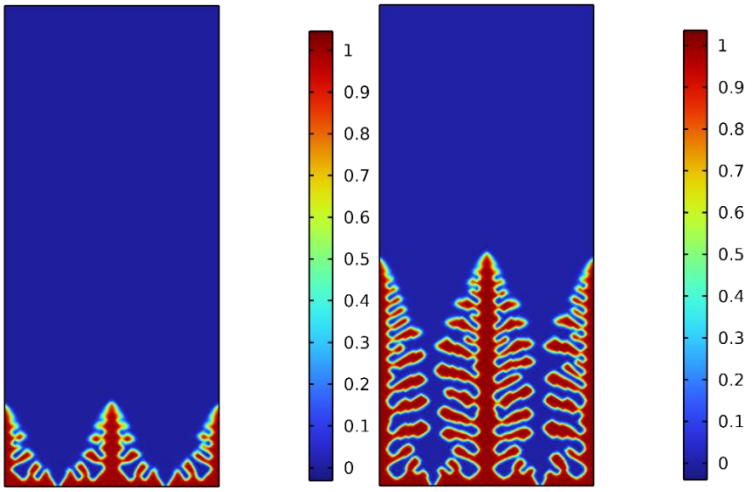

Figure 2. The normal growth process of dendrites within 3000Δ*t:* (**a**) dendrite morphology at 1000Δ*t*; (**b**) dendrite morphology at 3000Δ*t*.

After the evolution process reaches 3000Δ*t*, the ambient temperature around the dendrites increases, which causes the dendrites to melt, as shown in Figure 3. As shown in Figure 3a, it can be seen that at the 3005Δ*t* time step, parts of the lateral dendrites begin to melt, while the main dendrites show an obvious contraction trend. As shown in Figure 3b, with the continuation of the melting process, the overall growth of the dendrites stops, with some of the smaller lateral dendrites having completely melted, while the large lateral dendrites significantly decrease in width and length. As shown in Figure 3c, fracturing occurs at the root position of the lateral dendrites that have not been completely melted at 3030Δ*t*, and it can be seen that the main dendrite arm shows a significant contraction trend. As shown in Figure 3d, most of the lateral dendrites are completely melted at 3040Δ*t*, and the main dendrite arms also show clear signs of melting. As shown in Figure 3, during the remelting process, the main dendrite arms tend to shrink, and the stem width decreases.

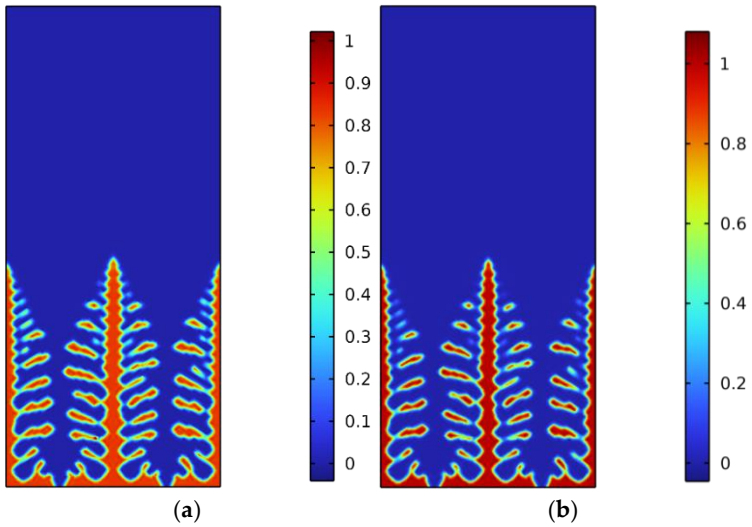

Figure 3. *Cont.*

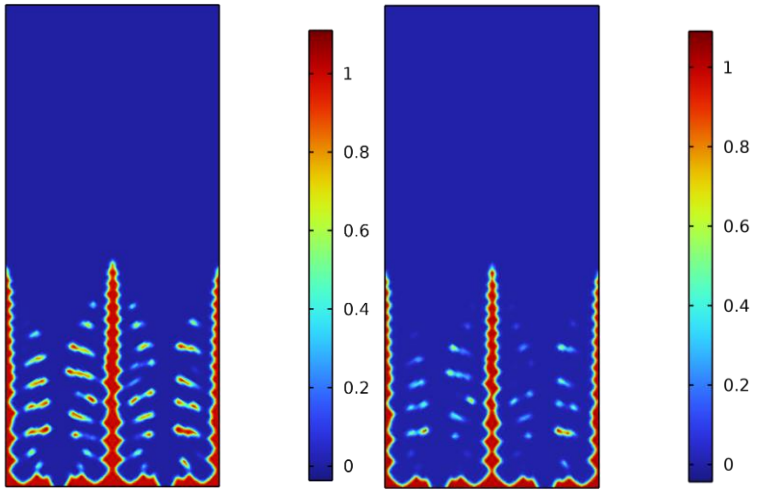

Figure 3. The process of the melting of grown dendrites after 3000Δ*t*: (**a**) dendrite morphology at 3005Δ*t*; (**b**) dendrite morphology at 3020Δ*t*; (**c**) dendrite morphology at 3030Δ*t*; (**d**) dendrite morphology at 3040Δ*t*.

3.2. Dendrite Remelting Mode in Lateral Dendrite Melting

As shown in Figure 3, during the remelting process, the main dendrite arms exhibit a shrinking trend, and the stem width decreases. The melting behavior of lateral dendrites can be categorized into two typical situations, as shown in Figures 4 and 5. The remelting effect caused by temperature rise and the capillary extrusion effect caused by interface curvature jointly act on the melting process of lateral dendrites. On the one hand, lateral dendrites tend to melt as a whole to maintain the thermodynamic equilibrium at the liquid–solid interface (L/S interface) [25]. On the other hand, the local interface energy difference caused by the negative curvature effect leads to significant capillary extrusion at the root of the lateral dendrites [26], which causes the lateral dendrites to break from the root. In the dendrite remelting process, these two effects compete with each other, resulting in two different melting behaviors of the lateral dendrites.

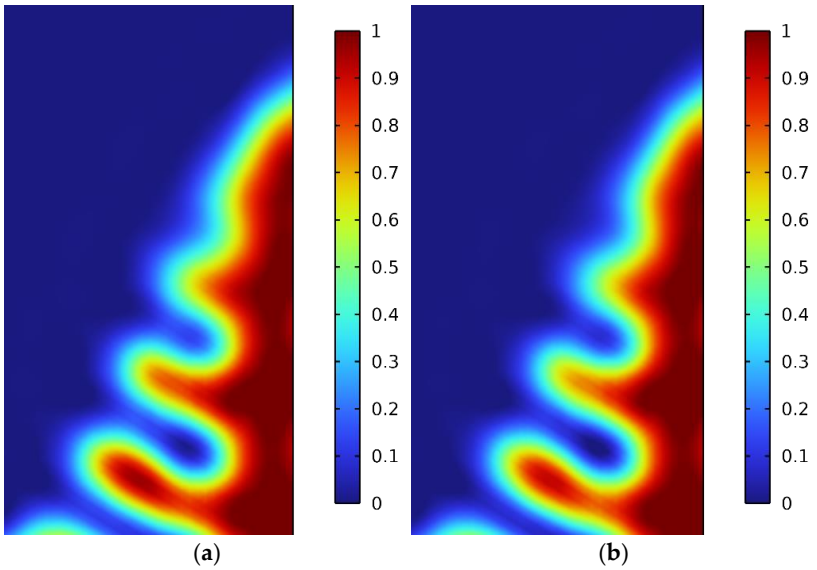

Figure 4. *Cont.*

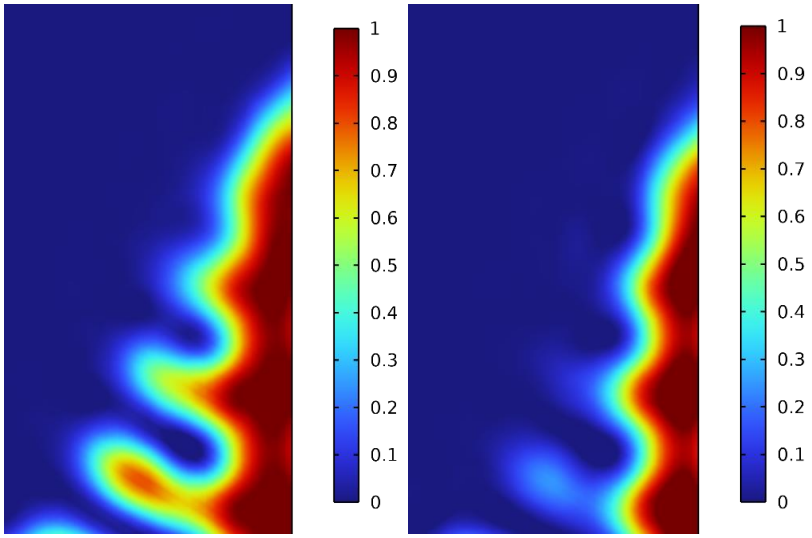

Figure 4. The phenomenon of lateral dendrites retracting into the main dendrite during the melting process. (**a**) Dendrite morphology at 3000Δt. (**b**) Dendrite morphology at 3002Δt. (**c**) Dendrite morphology at 3006Δt. (**d**) Dendrite morphology at 3018Δt.

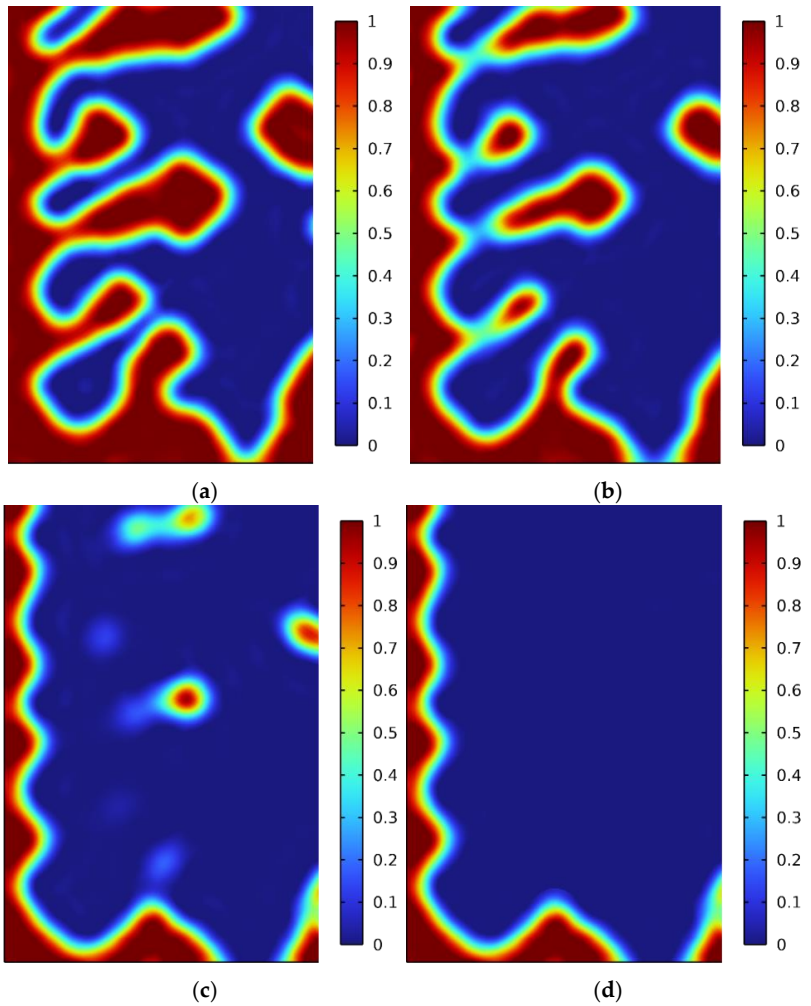

Figure 5. Truncation phenomenon during retraction of melted lateral dendrites. (**a**) Dendrite morphology at 3000Δt. (**b**) Dendrite morphology at 3000Δt. (**c**) Dendrite morphology at 3000Δt. (**d**) Dendrite morphology at 3000Δt.

As shown in Figure 4a–d, with the increase in ambient temperature, the stem morphology of the lateral dendrites becomes obviously "squeezed". The lateral dendrites melted before the root fracture until they contracted back into the main dendrites, without forming independent dendrite fragments. The second melting behavior is shown in Figure 5a–d. When the lateral dendrites melt to a certain extent, their roots fracture before completely shrinking back into the main dendrites and then form independent dendrite fragments. At the same time, it can be observed that after the lateral dendrite root fractures, due to the large surface free energy of the dendrite fragments during the melting process, their morphology gradually tends to transition toward a state of minimizing the surface energy. They finally present a nearly spherical melting morphology until completely melting. By observing the whole process of dendrite melting, it can be seen that the longer lateral dendrites show a more significant root fracture tendency, as shown in Figure 3a–d.

The difference between the two kinds of melting behavior reflects the complex competition between the local thermodynamic equilibrium and the capillary effect in the remelting process. In the first case, the thermodynamic equilibrium at the liquid–solid interface (L/S interface) is mainly maintained, and the lateral dendrites shrink from the root back into the main dendrite arm. The second case mainly reflects the influence of capillary compression at the root of the lateral dendrites caused by local interface energy differences caused by the negative curvature effect on lateral dendrite fracture behavior.

3.3. Dendrite Remelting—The Main Dendrite Melting Mode

As the melting process continued, the main dendrites entered the melting stage after the lateral dendrites fractured, as shown in Figure 6. It can be seen in Figure 6a that at $3050\Delta t$, the main dendrites begin to melt rapidly, and their width and length decrease significantly. As shown in Figure 6b, by the time the melting time step reaches $3070\Delta t$, the remaining collateral fragments have all melted into a liquid state. However, due to the heterogeneity in the local dendritic structure and the variability in the melting and fracturing behaviors of the lateral dendrites, the main dendrite fractures along the axial direction and finally splits into several smaller dendrite fragments. As shown in Figure 6c,d, the main dendrite undergoes complete melting between $3070\Delta t$ and $3100\Delta t$. At this stage, the entire dendritic structure has reverted to its initial crystal nucleus state, signifying the completion of the dendrite remelting process.

The dendrite melting process was comprehensively analyzed. As shown in Figures 4 and 6, the overall melting behavior of dendrites is manifested as the gradual melting and fracturing of lateral dendrites, followed by the main dendrites entering the melting stage. The main form of dendrite melting is distinguished by multi-segmented fracturing and melting. This multi-stage fracture behavior may be due to the microstructural characteristics of the main dendrites and the differences in the fracture processes of the lateral dendrites during melting. The complex melting behavior and structure evolution of dendrites during temperature rise has thus been revealed. Theoretical basis and data support have been provided to foster further understanding of the melting mechanism of dendrites under high-temperature conditions.

The above melting process is highly consistent with the experimental observation results obtained by Virkeshwar Kumar [27], indicating that that the numerical simulation presented in this paper can accurately reflect the morphological evolution and microstructure changes of dendrites during the remelting process. Thus, the reliability of the model-derived results has been verified.

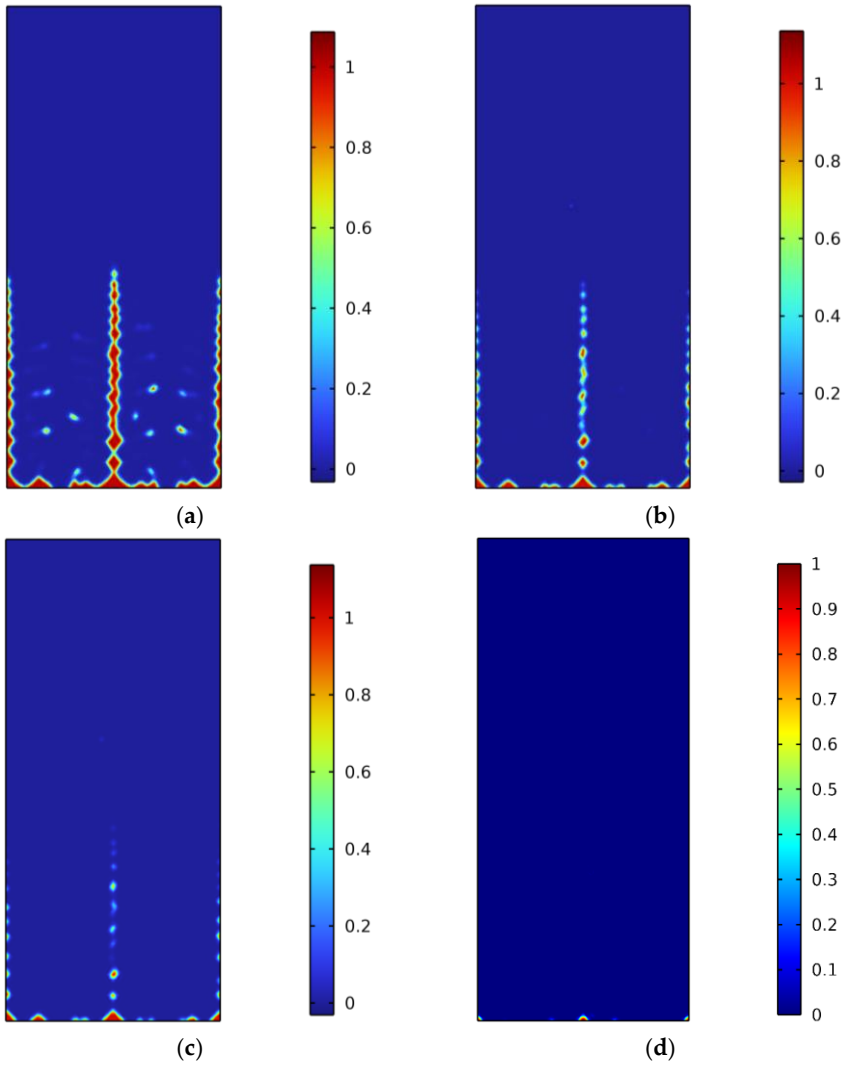

Figure 6. Melting of the primary dendrite arm after the melting of the secondary dendrite arm. (**a**) Dendrite morphology at 3050Δ*t*. (**b**) Dendrite morphology at 3050Δ*t*. (**c**) Dendrite morphology at 3050Δ*t*. (**d**) Dendrite morphology at 3050Δ*t*.

4. Conclusions

1. Based on the phase field method, a dendrite growth model was established and solved using the finite difference method (FDM), which provided the initial conditions for the solution of the dendrite remelting model. The results show that under the influence of interfacial anisotropy, the crystal nuclei exhibit obvious main dendrite growth in both horizontal and vertical directions, showing the characteristic of a preferred orientation in the process of dendrite growth.
2. Based on the solution data derived from the phase field method and dendrite growth model, a temperature-induced dendrite remelting model was established and solved. The results show that the dendrite remelting process follows a certain sequence, wherein the lateral branches melt the main dendrite first and then melt. When the lateral branches are not completely melted or the root is not broken, the main dendrite stem will shrink to a certain extent but not melt. The melting process of lateral branches consists of the contraction of lateral branches back into the main dendrites and the fracturing of the lateral branches of the main dendrites. The melting process of main dendrites takes the form of multi-stage melting due to the inhomogeneity of the crystal structure and the difference in the melting-induced fracturing of the lateral branches.

Author Contributions: X.H. and C.L. acquired the grant and revised the paper; H.Z. and S.L. performed modeling and wrote the paper; F.K. extracted and analyzed the data; J.L. and X.W. checked the grammar. All authors have read and agreed to the published version of the manuscript.

Funding: The Ministry of Science and Technology of the People's Republic of China provided funding via the following projects: "High-Throughput Design, Preparation, and Characterization of Composite Powders for Special Coatings on Key Components in Metallurgy" (2021YFB3702002); "Applied Basic Research Program of Liaoning Province" (2023JH2/101300226); "Project for Graduate Education Reform and Technological Innovation and Entrepreneurship of University of Science and Technology Liaoning" (2023YJSCX02); "Liaoning Province Metallurgical equipment and process control key laboratory open project fund (2024KFKT-01)"; "Supported by the Fundamental Research Funds for the Liaoning Universities (LJ222410146021)".

Institutional Review Board Statement: Not applicable.

Informed Consent Statement: Not applicable.

Data Availability Statement: The data that support the findings of this study are available within the article.

Conflicts of Interest: The authors declare no conflicts of interest.

References

1. Liu, S.; Ding, H.; Chen, R.; Guo, J.; Fu, H. Microstructural evolution and mechanical properties of a Cr-rich β-solidifying TiAl-based alloy prepared by electromagnetic cold crucible continuous casting. *Mater. Sci. Eng. A* **2020**, *798*, 140205. [CrossRef]
2. Zhi, Y.; Jiang, Y.; Ke, D.; Hu, X.; Liu, X. Review on Cellular Automata for Microstructure Simulation of Metallic Materials. *Materials* **2024**, *17*, 1370. [CrossRef] [PubMed]
3. Wang, J.; Wang, H.; Cheng, X.; Zhang, B.; Wu, Y.; Zhang, S.; Tian, X. Prediction of solidification microstructure of titanium aluminum intermetallic alloy by laser surface remelting. *Opt. Laser Technol.* **2022**, *147*, 107606. [CrossRef]
4. Rappaz, M.; Jarry, P.; Kurtuldu, G.; Zollinger, J. Solidification of metallic alloys: Does the structure of the liquid matter? *Metall. Mater. Trans. A* **2020**, *51*, 2651–2664. [CrossRef]
5. Yang, L.; Liu, L.J.; Qin, Q.Y.; Li, J.F. Role of remelting in grain refinement of undercooled single-phase alloys. *Metall. Mater. Trans. A* **2022**, *53*, 3100–3109. [CrossRef]
6. Ren, N.; Li, J.; Bogdan, N.; Xia, M.; Li, J. Simulation of dendritic remelting and fragmentation using coupled cellular automaton and Eulerian multiphase model. Computational. *Mater. Sci.* **2020**, *180*, 109714. [CrossRef]
7. Peng, X.L.; Xiao, H.; Li, W.H.; Yi, B.; Qin, W.; He, H. Simulation of Dendritic Morphology of Ni-Cu Alloy under Convection Based on Phase Field Method. *Shanghai Met.* **2021**, *43*, 69–76.
8. Rojas, R.; Sotomayor, V.; Takaki, T.; Hayashi, K.; Tomiyama, A. A phase field-finite difference lattice Boltzmann method for modeling dendritic growth solidification in the presence of melt convection. *Comput. Math. Appl.* **2022**, *114*, 180–187. [CrossRef]
9. Danilov, D.; Nestler, B. Phase-field simulations of solidification in binary and ternary systems using a finite element method. *J. Cryst. Growth* **2005**, *275*, e177–e182. [CrossRef]
10. Cha, P.R.; Yeon, D.H.; Yoon, J.K. A phase field model for isothermal solidification of multicomponent alloys. *Acta Mater.* **2001**, *49*, 3295–3307. [CrossRef]
11. Gonzalez-Cinca, R.; Folch, R.; Benitez, R.; Ramirez-Piscina, L.; Casademunt, J.; Hernandez-Machado, A. Phase-field models in interfacial pattern formation out of equilibrium. *arXiv* **2003**. [CrossRef]
12. Galfré, A.; Huang, X.; Couenne, F.; Cogné, C. The phase field method—From fundamentals to practical applications in crystal growth. *J. Cryst. Growth* **2023**, *620*, 127334. [CrossRef]
13. Plapp, M. Phase-field models. In *Handbook of Crystal Growth*; Elsevier: Amsterdam, The Netherlands, 2015; pp. 631–668. [CrossRef]
14. Zhu, C.; Jia, J.; Feng, L.; Xiao, R.; Dong, R. Research of three-dimensional dendritic growth using phase-field method based on GPU. *Comput. Mater. Sci.* **2014**, *91*, 146–152. [CrossRef]
15. Kavousi, S.; Gates, A.; Jin, L.; Zaeem, M.A. A temperature-dependent atomistic-informed phase-field model to study dendritic growth. *J. Cryst. Growth* **2022**, *579*, 126461. [CrossRef]
16. Liszka, T.; Orkisz, J. The finite difference method at arbitrary irregular grids and its application in applied mechanics. *Comput. Struct.* **1980**, *11*, 83–95. [CrossRef]
17. Zhang, Q.; Fang, H.; Xue, H.; Pan, S.; Rettenmayr, M.; Zhu, M. Interaction of local solidification and remelting during dendrite coarsening-modeling and comparison with experiments. *Sci. Rep.* **2017**, *7*, 17809. [CrossRef]
18. Kobayashi, R. Modeling and numerical simulations of dendritic crystal growth. *Phys. D Nonlinear Phenom.* **1993**, *63*, 410–423. [CrossRef]
19. Boettinger, W.J.; Warren, J.A.; Beckermann, C.; Karma, A. Phase-field simulation of solidification. *Annu. Rev. Mater. Res.* **2002**, *32*, 163–194. [CrossRef]

20. Zaeem, M.A.; Yin, H.; Felicelli, S.D. Modeling dendritic solidification of Al–3% Cu using cellular automaton and phase-field methods. *Appl. Math. Model.* **2013**, *37*, 3495–3503. [CrossRef]
21. Suzuki, T.; Ode, M.; Kim, S.G.; Kim, W.T. Phase-field model of dendritic growth. *J. Cryst. Growth* **2002**, *237*, 125–131. [CrossRef]
22. Acharya, R.; Sharon, J.A.; Staroselsky, A. Prediction of microstructure in laser powder bed fusion process. *Acta Mater.* **2017**, *124*, 360–371. [CrossRef]
23. Tong, X.; Beckermann, C.; Karma, A.; Li, Q. Phase-field simulations of dendritic crystal growth in a forced flow. *Phys. Rev. E* **2001**, *63*, 061601. [CrossRef] [PubMed]
24. Du, L.; Zhang, R. Phase field simulation of dendrite growth with boundary heat flux. *Integr. Mater. Manuf. Innov.* **2014**, *3*, 225–239. [CrossRef]
25. Sun, D.; Wang, Y.; Yu, H.; Han, Q. A lattice Boltzmann study on dendritic growth of a binary alloy in the presence of melt convection. *Int. J. Heat Mass Transf.* **2018**, *123*, 213–226. [CrossRef]
26. Chen, W.; Hou, H.; Zhang, Y.; Liu, W.; Zhao, Y. Thermal and solute diffusion in α-Mg dendrite growth of Mg-5wt.% Zn alloy: A phase-field study. *J. Mater. Res. Technol.* **2023**, *24*, 8401–8413. [CrossRef]
27. Kumar, V.; Karagadde, S.; Meena, K. Real-Time Strengthening of Natural Convection and Dendrite Fragmentation During Binary Mixture Freezing. In *Conference on Fluid Mechanics and Fluid Power*; Springer Nature: Singapore, 2022; pp. 691–700. [CrossRef]